applied sciences

MDPI

Article

Positional Isomeric Effects on the Physicochemical Properties of Polymeric Matrix and Polymer@TiO_2 Nanocomposites

Badria M. Al-Shehri [1], Amina Bekhoukh [2], Soumia Benkhatou [2], Imane Moulefera [3], Afaf Y. Khormi [1], Rabab A. Hakami [1], Magbool Alelyani [4], Jinan Abdelkader [5], Abdelghani Benyoucef [2,*] and Youssef Bakkour [4,*]

1 Department of Chemistry, Faculty of Science, King Khalid University, P.O. Box 9004, Abha 61413, Saudi Arabia
2 Water Science and Technology Laboratory, University of Mustapha Stambouli Mascara, Mascara 29000, Algeria; amina.bekhoukh@univ-mascara.dz (A.B.)
3 Chemical Engineering Department, Campus Universitario de Espinardo, University of Murcia, 30100 Murcia, Spain
4 Department of Radiological Sciences, College of Applied Medical Science, King Khalid University, Abha 61421, Saudi Arabia
5 Laboratory of Applied Chemistry, Faculty of Science III, Lebanese University, Tripoli 1352, Lebanon
* Correspondence: a.benyoucel@univ-mascara.dz (A.B.); ybakkour@kku.edu.sa (Y.B.)

Abstract: This study investigates the influence of positional isomerism on the physicochemical characteristics of polymeric matrices by examining polyo-anisidine (POA) and polyp-anisidine (PPA) in conjunction with TiO_2 nanoparticles. The synthesis of POA@TiO_2 and PPA@TiO_2 involved chemical oxidative polymerization. X-ray diffraction analysis revealed the anatase structure of TiO_2 nanoparticles. Transmission electron microscopy confirmed the successful integration of TiO_2 nanoparticles within the polymer matrix. Moreover, FTIR and UV–Vis spectroscopy confirmed the effective interaction between the nanoparticle and the polymer. TGA indicated that POA@TiO_2 exhibited a lower weight loss than PPA@TiO_2, suggesting an enhancement in thermal stability. Although the incorporation of TiO_2 nanoparticles led to a reduction in the electrical conductivity of the pristine polymers (PPA and POA), the resultant nanocomposites retained high conductivities within the range of 0.08 to 0.34 $S.cm^{-1}$. Furthermore, the POA-based polymer matrix displayed promising electrochemical properties. Significantly, the adherence of the POA layer to TiO_2 nanoparticles suggests potential practical applications.

Keywords: poly(o-anisidine); poly(p-anisidine); titanium dioxide; isomers; electrochemical properties

Citation: Al-Shehri, B.M.; Bekhoukh, A.; Benkhatou, S.; Moulefera, I.; Khormi, A.Y.; Hakami, R.A.; Alelyani, M.; Abdelkader, J.; Benyoucef, A.; Bakkour, Y. Positional Isomeric Effects on the Physicochemical Properties of Polymeric Matrix and Polymer@TiO_2 Nanocomposites. *Appl. Sci.* **2024**, *14*, 2106. https://doi.org/10.3390/app14052106

Academic Editor: Leonarda Liotta

Received: 31 January 2024
Revised: 22 February 2024
Accepted: 27 February 2024
Published: 3 March 2024

1. Introduction

Conducting polymers (CPs) play an important role in material nanoscience and technology [1] due to their exceptional characteristics and versatile applications. These polymers are characterized by polyconjugated structures, which endow them with distinct electrical properties and stability, setting them apart from conventional polymers [1]. These polyconjugated structures have revolutionized the development of various electronic and electrochemical devices, leading to widespread applications in diverse areas [2], including metallic coatings, diodes, sensors, and microelectronic devices [2–4].

The continuous advancement of CPs and nanocomposites has brought attention to the impact of isomeric functional groups on their properties, highlighting the need for in-depth investigations in this area. Understanding how the positioning of functional groups within isomeric polymers affects their behavior and characteristics is crucial for optimizing their performance in various technological applications. They have an essential role in the domain of material science and technology [1]. Polyconjugated structures present in conducting polymers are widely used to determine electrical properties and their stability, which are unique to other conventional polymers [1].

Among the different types of conducting polymers, polyaniline (PAni) and polypyrrole, along with their derivatives, hold particular significance in both academic research and industrial applications [5]. These polymers exhibit a unique combination of electrical conductivity, mechanical flexibility, and chemical stability, making them highly desirable for a wide range of technological advancements. Researchers have extensively explored their properties and functionalities, paving the way for their integration into various cutting-edge technologies.

Given their ability to conduct electricity, these polymers have found use in the development of rechargeable batteries, contributing to the ongoing quest for more efficient and sustainable energy storage solutions. Moreover, their application to metallic coatings has facilitated the production of corrosion-resistant materials, enhancing the durability and longevity of various industrial components. Additionally, their role in the field of sensors has enabled the creation of highly sensitive and selective devices for detecting a wide range of substances and environmental changes. Furthermore, their integration into diodes, transistors, and microelectronic devices has revolutionized the landscape of modern electronics, enabling the development of smaller, faster, and more efficient electronic components. Continuous research and development in this field has not only expanded the fundamental understanding of conducting polymers but has also facilitated the development of novel materials with enhanced properties and functionalities. As a result, conducting polymers continue to be a key area of focus for scientists and engineers, driving innovation and progress in the realm of material nanoscience and technology.

Anisidine is a compound with a methoxy-aromatic amine group (methoxy aniline), considered a pollutant decomposition product of azo dyes. The methoxy (-OCH_3) group position has been specified between the three isomers of ortho-, meta-, and para-anisidines [6]. It is inexpensive and has good solubility in water [7]. Additionally, poly(o-anisidine) is a polyaniline derivative with high stability and good mechanical properties. However, regarding human health hazards, it is classified as an inhalation toxicant due to its ability to form methemoglobin associated with humans and found in cats [6]. On the other hand, poly (P-anisidine) is a polyaniline isomer that increases a material's specific capacitance and presents high stability as well as poly(o-anisidine) due to the methoxy group. Both polymers exhibit interesting characteristics such as high surface areas, electrochemical stability, and excellent redox [1].

Over the past decades, semiconductor photocatalysis has attracted considerable attention as an affordable and uncomplicated technology for wastewater treatment. Thus, extensive research has been conducted on nanostructured metal-oxide (MO) semiconductors such as TiO_2 [8,9]. Despite being one of the more commonly employed photocatalytic materials [10], TiO_2 has a relatively wide band gap ranging from 3.0 to 3.3 eV [8,11]. As a result, bare TiO_2 only exhibits photoactivity under UV excitation, making it a disadvantage from this perspective. For this reason, researchers are exploring and developing TiO_2-based photocatalyst systems with an improved visible-light response [10,11]. This effect has been obtained by coupling conducting polymers (PCs) with TiO_2 photocatalysts, improving TiO_2 photocatalytic efficiency [8,12]. However, conjugated polymers and their derivatives can act as photosensitizers and have shown excellent stability due to their extending π-conjugated electron systems. Therefore, the synergistic impact of combining these two types of materials (CPs and TiO_2) to create a composite (CP@TiO_2) may enhance one another and improve photocatalysis features including stability, quick reaction, and recovery [13]. On the other hand, pure TiO_2 is typically considered an insulating material that is known for its high surface area. Hence, incorporating TiO_2 into a CP matrix can lead to synergistic effects and increase the available surface area for electrolyte interactions, potentially improving charge storage and increasing electrical conductivity and electrochemical properties [14]. Understanding the interplay between phase structure and TiO_2 addition is crucial for tailoring materials to meet specific requirements in photocatalyst and energy storage applications.

The main objectives of this work are to highlight the important role of a functional group's position in isomers for polymer and nanocomposite properties, as well as to characterize the final composite obtained by doped isomers with TiO_2 oxide such as FTIR, XRD, diffraction, TG analysis, and electrochemical properties.

2. Materials and Methods

2.1. Materials and Chemicals

The two isomers of anisidine (monomers), P-Anisidine (PA) and O-Anisidine (OA) (from Aldrich, Madrid, Spain.), were used as received. Chemicals such as perchloric acid ($HClO_4$, 70% purity), hydrochloric acid (HCl, 37% purity), titanium (IV) oxide (TiO_2, 99.98% purity), ammonium persulfate (APS, 98% purity), N-methyl-2-pyrrolidone (NMP), and ammonia solution (NH_4OH, 25% purity) used in this work were of analytical purity and supplied by Merck KGaA (Darmstadt, Germany). The ultrapure water used in all the experiments was obtained from the Elga-Lab Water-Pure lab system.

2.2. Chemical Synthesis of Hybrid Materials

The two polymers (PPA and POA) and their corresponding nanocomposites with TiO_2, PPA@TiO_2, and POA@TiO_2 were prepared via chemical oxidation [15–17]. Firstly, the desired TiO_2 was dispersed in (1M) HCl under magnetic stirring for 30 min to activate the surface of TiO_2 nanoparticles. Afterward, 0.25 mol of PA or OA monomers were prepared and preserved at room temperature in HCl. We added 0.5 g of a TiO_2-activated mass to the previous solution, stirred it for 1 h to obstruct nanoparticle agglomeration, and allowed the electrostatic interaction to deposit monomers onto the TiO_2 surface. Then, an APS (1M) was added dropwise at room temperature for 24 h. Afterward, the precipitates were placed in 50 mL of NH_4OH (1M) at 25 °C while stirring for 2 h. Finally, the resultant mixtures were filtered, rinsed several times with H_2O, and dried for 24 h at 65 °C [15,18,19].

Figure 1 depicts the polymerization process of PPA@TiO_2 and POA@TiO_2 nanocomposites [20]. In an acidic environment, the surface charge of TiO_2 becomes positive, causing Cl^- ions to adhere to the nanoparticle surface to balance the positive charges. Simultaneously, the monomers (PA or OA) undergo transformation into cationic anilinium ions under the same acidic conditions. This process causes electrostatic attraction between the Cl^- ions attached to the surface and the cationic anilinium ions.

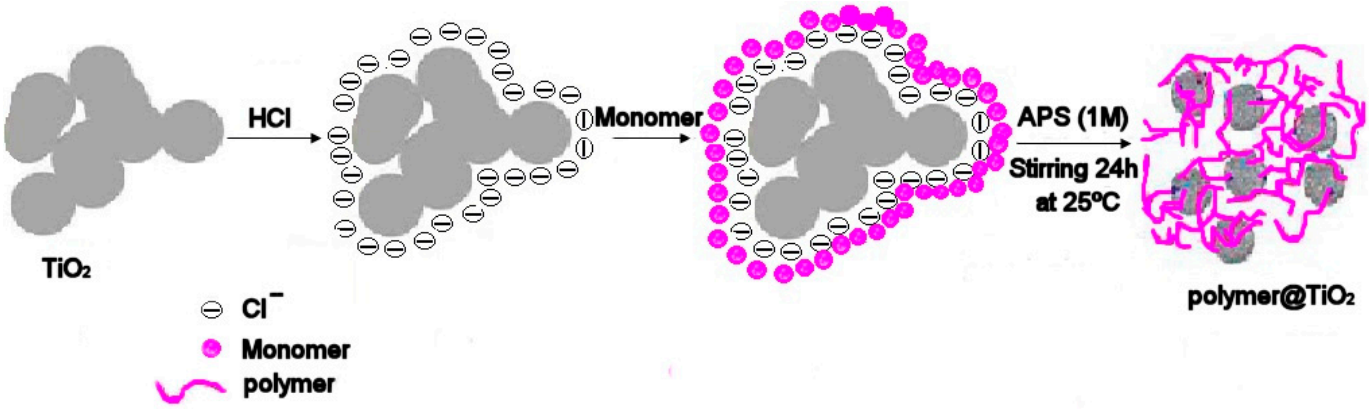

Figure 1. Schematic representation of polymer@TiO_2 nanocomposite preparation.

2.3. Physicochemical Characterization

The crystal structures of the prepared samples were studied using a Bruker CCD-Apex (Madison, WI, USA) model X-ray diffractometer (XRD). The specific micromorphology of the samples was observed by transmission electron microscopy (JEOL-JEM-2010; Peabody, MA, USA). A Hitachi U-3000 spectrophotometer was used to obtain UV–visible spectra. A Bruker–Alpha spectrophotometer (Varian, Inc., Palo Alto, CA, USA) was used to measure FT–IR and evaluate the functional units of the samples. A Hitachi STA–7200 instrument

(Fukuoka, Japan) was used to perform thermogravimetric analysis (TGA) under nitrogen. About 10 mg of nanocomposites were heated to 900 °C with a heating rate of 20 K.min^{-1} [18,19].

2.4. Electrochemical Analyses

We studied the electrochemical behavior of the samples using cyclic voltammetry (CV). The material was initially dissolved in NMP. Subsequently, the dissolved polymers were extracted from the nanocomposites [15]. Afterward, a small volume of the resultant solution was deposited onto a glassy carbon electrode with a geometrical area of 0.07 cm^2. The solution was dried using an infrared lamp to eliminate NMP. Electrochemical tests were conducted with a conventional 3–electrode cell setup. RHE (reversible hydrogen electrode) and platinum (Pt) were employed as reference and counter electrodes, respectively. A 1M solution of $HClO_4$ was used as the electrolyte for all experiments, which were performed at a 50 mV.s^{-1} scan rate.

2.5. Electrical Conductivity Characterization

We used LucasLab resistivity equipment (Rochester, NY, USA) with 4-in-line probes to perform conductivity assessments. Before taking measurements, the materials underwent a drying process for 24 h. Pellets, each possessing a diameter of 0.013 cm, were fashioned using a mold of FTIR. These pellets were created by subjecting the materials to a pressure of 7.4 $\times$ 10^8 Pa.

3. Results and Discussion

3.1. FTIR Analysis

Figure 2a displays the FTIR spectra of TiO_2 nanoparticles, POA, PPA, POA@TiO_2, and PPA@TiO_2. The locations of characteristic bands associated with the respective chemical bonds are summarized in Table 1.

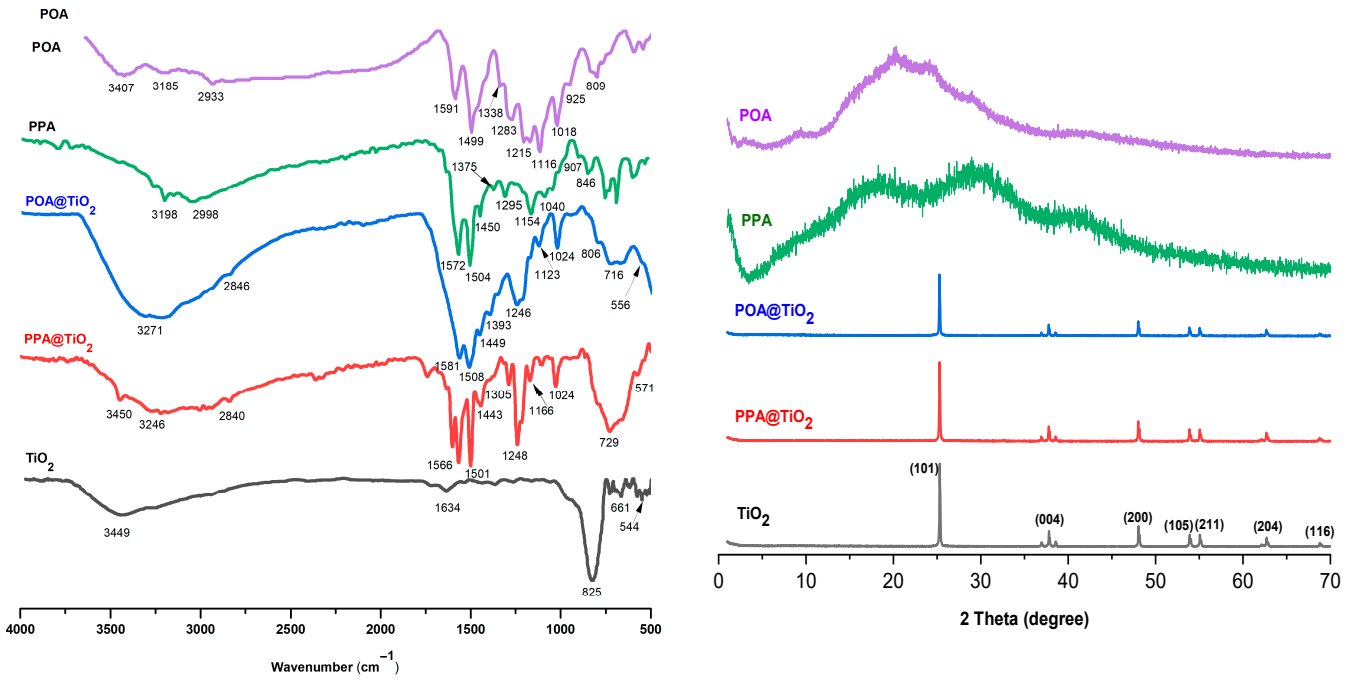

(**a**) (**b**)

Figure 2. (**a**) FTIR analysis and (**b**) XRD powder diffraction patterns of TiO_2 nanoparticles and PPA, POA, POA@TiO_2, and PPA@TiO_2 nanocomposites.

Table 1. IR peaks of TiO_2 nanoparticles and PPA, POA, POA@TiO_2, and PPA@TiO_2 nanocomposites.

Peak Assignment	POA	PPA	POA@TiO_2	PPA@TiO_2	TiO_2
–NH Stretching vibrations	3185	3198	3271	3246	//
–CH Stretching vibrations	2933	2998	2846	2840	//
Quinonoid	1591	1572	1581	1566	//
Benzenoid	1499	1504	1508	1501	//
–C–N	1338	1375	1393	1305	//
B–N^+H–B & Q=N^+H–B	1018	1040	1024	1024	//
C–O aromatic	1116	1154	1123	1166	//
CH_3 group	1418	1450	1449	1443	//
C–O–C	1283	1295	1246	1248	//
TiO	//	//	716–556	729–571	825–544

The bands of TiO_2 nanoparticles are associated as follows: the band at 3449 cm^{-1} is ascribed to stretching vibrations of the surface OH^- or adsorbed H_2O molecules; a band at 1634 cm^{-1} can be assigned to a vibration of –OH on the surface of TiO_2, and the bands at 825 cm^{-1} and 661 cm^{-1} are due to Ti–O stretching modes [21].

The results in Table 1 demonstrate some differences between PPA and POA. The IR spectrum of pure POA exhibited a characteristic absorption band at 3185 cm^{-1} due to N–H stretching vibrations [22–24]. The bands at 2933 cm^{-1} are indicative of C–H stretching vibrations [25]. The two bands at 1591 cm^{-1} and 1499 cm^{-1} correspond to the quinoid and benzenoid groups, respectively [26,27]. The band at 1116 cm^{-1} is associated with C–O aromatics [12]. Moreover, a band appearing at 1418 cm^{-1} may be due to the presence of a CH_3 group or aromatic characteristics [28]. The band observed at 1283 cm^{-1} can be attributed to the C–O–C vibrations of the ether group [12,29]. Additionally, the bands observed at 1146 cm^{-1} and 1338 cm^{-1} may be related to C–N and C=N stretching modes [22,30]. The band at 1018 cm^{-1} corresponds to the 1–4 substitution on the benzene ring [26,27] and the bands at 925 cm^{-1} and 809 cm^{-1} may be due to the C–H out–plane bending vibrations of 1,2,4 trisubstituted aromatic rings [23]. Therefore, these distinctive spectral features confirmed successful POA formation by FTIR spectroscopic analysis.

The findings presented in Table 1 highlight notable disparities between PPA and POA, notably in the position and intensity of their respective bands. IR spectra reveal that POA@TiO_2 and PPA@TiO_2 nanocomposites exhibit the principal characteristic bands found in pure polymers (POA and PPA). However, the discernible shift in all bands suggests an interaction between pure polymers and TiO_2. Moreover, the presence of Ti–O bands between 716 cm^{-1} and 556 cm^{-1} in the FTIR spectra of nanocomposites serves as definitive evidence of the successful integration of TiO_2 into the polymer matrix. This finding substantiates the notion of a chemical interaction occurring between TiO_2 nanoparticles and the polymer structure, influencing spectral characteristics and affirming their amalgamation within composite materials [28,31].

3.2. XRD Analysis

The XRD patterns depicted in Figure 2b illustrate the XRD analyses of the POA polymer, PPA polymer, TiO_2 nanoparticles, and PPA/TiO_2, POA/TiO_2 nanocomposites. The XRD pattern of PPA and POA conducting polymers exhibits a broad peak around 2θ (20°–30°). This specific value indicates an amorphous nature [30], possibly attributed to polymer chains scattering at interplanar spacings [23].

The XRD of both the POA@TiO_2 and PPA@TiO_2 nanocomposites was compared to those of the polymers (PPA and POA) and revealed distinct features. Notably, prominent peaks were observed at 2θ values of 25.28°, 36.9°, 37.81°, 38.57°, 48.05°, 53.85°, 55.03°, 62.12°, 62.69°, and 68.76° and were ascribed to the (101), (103), (004), (112), (200), (105), (211), (204), and (116) crystal planes of anatase TiO, respectively [28,32]. These findings decisively confirm the presence of TiO_2 within both POA and PPA matrices. The XRD analysis also indicated that TiO_2 retains its structural integrity even after dispersion within the polymer matrix following the polymerization process [28]. Additionally, a small, low-intensity peak

around 32°, observed specifically in the hybrid material, likely corresponds to the presence of polymer@TiO_2 materials via a chemical oxidation method [21], further supporting the successful integration and structural integrity of the hybrid materials.

3.3. Electrical Conductivity (EC)

The EC of polymers hinges significantly on the mobility and quantity of charge carriers, closely linked to the material's morphology and chemical composition. Factors such as type, crystallinity degree, and tactile properties are pivotal in evaluating polymers' electrical traits [33,34]. EC was determined for all products that underwent the previously described experimental conditions; the results are displayed in Table 2. As shown in Table 2 the polymer solids exhibited notably high conductivity at standard room temperature. Specifically, the POA sample displayed a conductivity of approximately 0.34 $S{\cdot}cm^{-1}$, whereas the PPA sample showed a lower conductivity of 0.22 $S{\cdot}cm^{-1}$. This discrepancy confirms that the PPA sample holds the least concentration of emeraldine salts, whereas the POA boasts the highest concentration. However, the introduction of nanocomposites resulted in a considerable decrease in conductivity levels. This reduction primarily stems from stereochemical variations among these nanocomposites.

Table 2. The EC values of POA, PPA, and PPA@TiO_2, POA@TiO_2 nanocomposites.

Samples	PPA@TiO_2	POA@TiO_2	PPA	POA
EC ($S.cm^{-1}$)	0.08	0.09	0.22	0.34

The oxidized polymer displayed an almost linear structure, contributing to a minimal ionization potential because of the robust delocalization of electrons. This structural characteristic significantly impacts its conductivity. In this context, the decline in conductivity of nanocomposites suggests that the presence of TiO_2 nanoparticles hampers or disrupts electron transportation pathways within the polymers. This interference likely occurs by potentially diminishing the length of polymer chains, which affects the material's overall conductivity.

3.4. UV–Visible Analysis

Figure 3a presents the UV–visible spectra of POA, PPA, and PPA@TiO_2, POA@TiO_2 nanocomposites, where these materials were dissolved in an NMP solution. The three samples show two peaks: A peak near 298–378 nm, which can be attributed to transitions in the benzenoid structure [35,36], and a peak around 452–530 nm, which may correspond to quinine–imine group transitions [36,37]. These results reveal that polymer deprotonation by NH_4OH forms emeraldine bases [38].

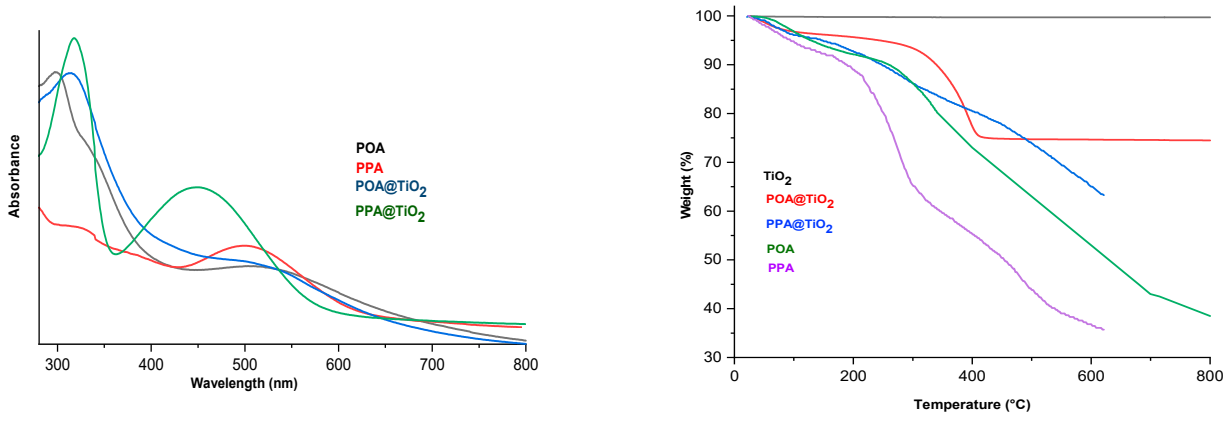

(**a**) (**b**)

Figure 3. (**a**) UV–Vis spectra of samples; (**b**) TGA analysis of TiO_2, POA, PPA, POA@TiO_2 and PPA@TiO_2 nanocomposites.

Intense band changes after inserting TiO_2 nanoparticles and a notable redshift of the peaks were observed for pure polymers compared to nanocomposites. The redshift distribution of POA@TiO_2 was larger than PPA@TiO_2 likely due to interchain species, which profoundly impact the conjugated polymers' process [28]. These results are in accord with nanocomposites' decreased conductivity (various transitions are included in Table 3). The continuous variation in the UV–visible peaks' wavelength and intensity confirms the interaction between polymers and nanoparticles.

Table 3. Absorption bands and redox peaks of prepared materials.

Materials	Redox Peak (V)						Absorption Band (nm)	
	E_{pa1}	E_{pc1}		E_{pa2}	E_{pc2}			
PPA	0.40	0.36	0.04	0.74	0.71	0.03	328	503
POA	0.41	0.30	0.11	0.67	0.51	0.16	298	530
POA@TiO_2	0.45	0.28	0.17	0.67	0.56	0.11	314	512
PPA@TiO_2	0.43	0.33	0.10	/	/	/	318	452

3.5. TGA Analysis

In this work, TGA analysis was used to test the thermal stability of TiO_2 nanoparticles, POA, PPA, POA@TiO_2, and PPA@TiO_2. The TGA profiles as a function of temperature in all synthesized materials are shown in Figure 3b.

The TGA curve of TiO_2 presents minor weight loss below 450 °C, which can be associated with the elimination of H_2O, ethanol, and partial dihydroxylation of TiO_2 nanoparticles [12].

The TGA of all samples underwent four weight loss steps. An initial weight loss (5%) at temperatures over 120 °C was attributed to the evaporation of entrapped H_2O, solvent, and monomers in the samples [39–41]. The second step of decomposition takes place at 160 °C to 450 °C and corresponds to the elimination of the oxidant. The third step of weight loss was observed in the range of 300 °C–500 °C and attributed to the removal of the acid dopant. Finally, the complete decomposition of polymer chains began near 500 °C and continued up to 630 °C for PPA and its nanocomposite PPA@TiO_2 [41]. By contrast, it was 700 °C for POA, and even after 700 °C, total decomposition did not occur [42]. POA@TiO_2 showed lower weight loss between 410 °C and 800 °C and the residue remaining in this zone provided an approximate estimate of filler content.

Moreover, at temperatures up to 600 °C, 62.5% of the PPA and 47% of the POA had decomposed. The POA@TiO_2 nanocomposite presented greater thermal stability with a total mass loss of 25%. By contrast, PPA@TiO_2 presented a higher mass loss of 32%. These results indicate that the interaction between the TiO_2 particles and polymer chains may have limited the thermal motion of TiO_2 particles and provided thermal stability to nanoparticles [43].

The weight mass loss of the three prepared polymeric samples displayed finite differences in their thermogravimetric analysis, indicating a minor decrease in the polymers' weight mass loss compared to nanocomposites. Therefore, the nanocomposites' thermal degradation presents higher stability than polymers. Additionally, the results show that the TGA curve of POA@TiO_2 lost less weight than the PPA@TiO_2 nanocomposite.

3.6. Electrochemical Study

CV was performed to test the polymers' electroactivity. Figure 4 shows the CV curves of PPA, POA, POA@TiO_2, and PPA@TiO_2 materials obtained in $HClO_4$ (1M) at 50 $mV.s^{-1}$ scan rate. Regarding POA, three overlapping redox processes were observed. The first occurred at 0.45/0.20 V and resulted in a potential peak separation (E_p) of 250 mV. Another redox pair at 0.86/0.74 V presented an E_p close to 120 mV. This redox process was assigned to the leucoemeraldine/emeraldine and emeraldine/pernigraniline transitions, respectively [23,30].

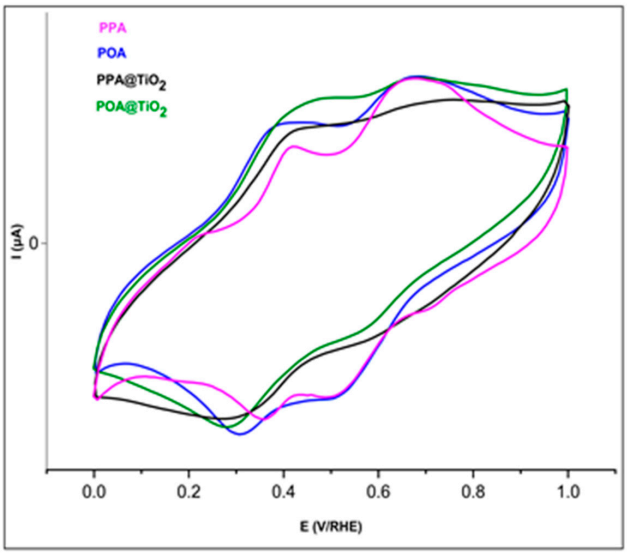

Figure 4. CV recorded on glassy carbon electrode modified by synthesis samples in $HClO_4$ (1 M) at a 50 $mV.s^{-1}$ scan rate.

The POA had similar CV shapes and peak potentials to the POA@TiO_2 nanocomposite; however, the peak pairs were shifted to higher potentials and lower intensity. The CV profile of the PPA@TiO_2 nanocomposite shows a unique redox process corresponding to 0.43/0.33 V and E_p = 100 mV, which corresponds to the leucoemeraldine/pernigraniline reaction [15]. Therefore, CV results may have been due to an earlier (lower) POA oxidation potential, i.e., higher POA reactivity than PPA [39]. Additionally, the anodic and cathodic peaks of PPA were symmetrical ($E_{P/2C} = E_{P/2a}$), indicating that the relevant redox events were highly reversible [40]. This reversible system corresponds to the p-doping of the polymer (oxidized) and n-doping of the polymer (reduced) represented by the oxidation wave and reduction wave, respectively. These findings show that the electrochemical properties of anisidine isomers depend on functional groups' (-OCH_3) relative position to one another, their arrangement in the polymer chain, and the existence of metal oxides in the polymer matrix.

3.7. TEM Analyses

Figure 5 displays TEM images of TiO_2 nanoparticles and POA@TiO_2 and PPA@TiO_2 nanocomposites. TiO_2 presents an almost spherical shape and uniform nanoparticle size with a diameter of about 100 nm, similar to those reported in the literature [44–46]. Moreover, all products had a spherical morphology, which was likely induced by absorbing monomers on the surface of TiO_2 through H-bonding and electrostatic attraction after HCl acidified the TiO_2 spheres. The TiO_2 surface was modified during the acidification stage, and no other surface treatments were necessary [43]. Moreover, TEM images of the nanocomposites indicate that TiO_2 particles were successfully dispersed into the polymer matrix [47].

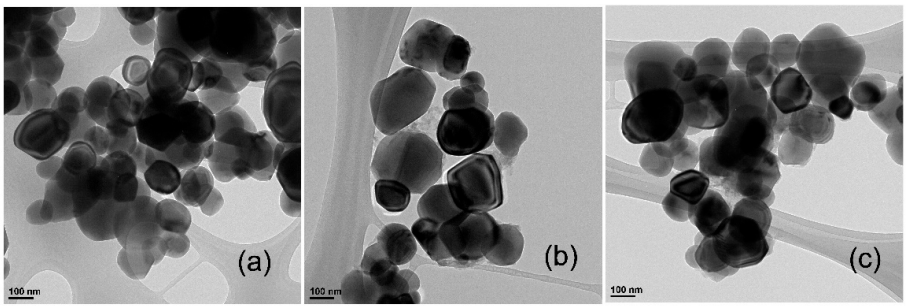

Figure 5. TEM images of (**a**) TiO_2 nanoparticle; (**b**) PPA@TiO_2, and (**c**) POA@TiO_2 nanocomposites.

4. Conclusions

In this study, two polymers incorporating the positional isomers para-anisidine (PPA) and ortho-anisidine (POA), along with their respective polymer@TiO_2 nanocomposites, were prepared via in situ chemical oxidation with HCl as a dopant and APS as an oxidant. The physicochemical properties of all samples were influenced by positional isomeric differences. Significantly, POA demonstrated higher electrical conductivity and favorable electrochemical responses. Various analytical techniques, including XRD, TEM, FTIR, and UV–visible spectroscopy, confirmed the successful integration of TiO_2 into the polymer matrix. This confirmation was evident through observed shifts in the peaks and bands within the spectra, indicating interactions between nanoparticles and the polymer. TGA revealed that the presence of nanocomposites improved the thermal stability of the polymers. Additionally, the electrochemical characteristics of POA@TiO_2 outperformed those of PPA@TiO_2.

Author Contributions: Conceptualization: B.M.A.-S., A.B. (Amina Bekhoukh), S.B. and I.M.; methodology: B.M.A.-S., A.B. (Amina Bekhoukh), S.B., I.M. and A.B. (Abdelghani Benyoucef); software: B.M.A.-S., A.B. (Amina Bekhoukh), S.B. and I.M.; validation: A.B. (Amina Bekhoukh), S.B., J.A. and A.B. (Abdelghani Benyoucef); visualization: A.B. (Amina Bekhoukh), S.B. and I.M.; formal analysis: A.B. (Amina Bekhoukh), A.Y.K., R.A.H., J.A. and A.B. (Abdelghani Benyoucef); investigation: A.B. (Amina Bekhoukh), J.A., M.A., Y.B. and A.B. (Abdelghani Benyoucef); data curation: B.M.A.-S., A.B. (Amina Bekhoukh) and Y.B.; writing—original draft preparation: B.M.A.-S., A.B. (Amina Bekhoukh), S.B., A.B. (Abdelghani Benyoucef) and Y.B.; supervision, A.B. (Abdelghani Benyoucef) writing, review and editing: B.M.A.-S., A.B. (Amina Bekhoukh), S.B., Y.B. and A.B. (Abdelghani Benyoucef). All authors have read and agreed to the published version of the manuscript.

Funding: This work was funded by the Deanship of Scientific Research at King Khalid University under grant number RGP2/358/44. The APC was also funded by King Khalid University.

Institutional Review Board Statement: Not applicable.

Informed Consent Statement: Data are contained within the article.

Data Availability Statement: The datasets used in the current study are available from the corresponding author upon reasonable request.

Acknowledgments: The Deanship of Scientific Research at King Khalid University financially supported this work through Grant No. RGP2/358/44. Moreover, the authors also want to thank their parental universities for providing the facilities to accomplish this investigation.

Conflicts of Interest: The authors declare no conflict of interest.

References

1. Rathidevi, K.; Velmani, N.; Tamilselvi, D. Electrical conductivity study of poly(p-anisidine) doped and undoped ZnO nanocomposite. *Mediterr. J. Chem.* **2019**, *9*, 403–410. [CrossRef]
2. MacDiarmid, A.; Yang, L.; Huang, W.; Humphrey, B. Polyaniline: Electrochemistry and application to rechargeable batteries. *Synth. Met.* **1987**, *18*, 393–398. [CrossRef]
3. Martins, J.; Reis, T.; Bazzaoui, M.; Bazzaoui, E.; Martins, L. Polypyrrole coatings as a treatment for zinc-coated steel surfaces against corrosion. *Corros. Sci.* **2004**, *46*, 2361–2381. [CrossRef]
4. Sukeerthi, S.; Contractor, A. Applications of conducting polymers as sensors. *Indian J. Chem.-Sect. A* **1994**, *33*, 565–571.
5. Paul, E.W.; Ricco, A.J.; Wrighton, M.S. Resistance of polyaniline films as a function of electrochemical potential and the fabrication of polyaniline-based microelectronic devices. *J. Phys. Chem.* **1985**, *89*, 1441–1447. [CrossRef]
6. Sharma, R.; Dave, S. Electrochemical Studies of o- and p-Anisidine. *Int. J. Appl. Sci. Biotechnol.* **2015**, *3*, 267–271. [CrossRef]
7. Chaudhari, S.; Gaikwad, A.; Patil, P. Poly(o-anisidine) coatings on brass: Synthesis, characterization and corrosion protection. *Curr. Appl. Phys.* **2009**, *9*, 206–218. [CrossRef]
8. Coromelci, C.G.; Turcu, E.; Doroftei, F.; Palamaru, M.N.; Ignat, M. Conjugated Polymer Modifying TiO_2 Performance for Visible-Light Photodegradation of Organics. *Polymers* **2023**, *15*, 2805. [CrossRef]
9. Katančić, Z.; Chen, W.-T.; Waterhouse, G.I.; Kušić, H.; Božić, A.L.; Hrnjak-Murgić, Z.; Travas-Sejdic, J. Solar-active photocatalysts based on TiO2 and conductive polymer PEDOT for the removal of bisphenol A. *J. Photochem. Photobiol. A Chem.* **2020**, *396*, 112546. [CrossRef]

10. Samsudin, E.M.; Hamid, S.B.A. Effect of band gap engineering in anionic-doped TiO_2 photocatalyst. *Appl. Surf. Sci.* **2017**, *391*, 326–336. [CrossRef]
11. Ignat, M.; Rotaru, R.; Samoila, P.; Sacarescu, L.; Timpu, D.; Harabagiu, V. Relationship between the component synthesis order of zinc ferrite–titania nanocomposites and their performances as visible light-driven photocatalysts for relevant organic pollutant degradation. *Comptes Rendus Chim.* **2018**, *21*, 263–269. [CrossRef]
12. Zhou, Q.; Shi, G. Conducting Polymer-Based Catalysts. *J. Am. Chem. Soc.* **2016**, *138*, 2868–2876. [CrossRef]
13. Dimitrijevic, N.M.; Tepavcevic, S.; Liu, Y.; Rajh, T.; Silver, S.C.; Tiede, D.M. Nanostructured TiO_2/Polypyrrole for Visible Light Photocatalysis. *J. Phys. Chem. C* **2013**, *117*, 15540–15544. [CrossRef]
14. Kailasa, S.; Reddy, M.S.B.; Rani, B.G.; Rao, K.V.; Deshmukh, K.; Sadasivuni, K.K. Highly sensitive electrochemical volatile organic compound (Acetone) sensing based on TiO_2 Nanocubes @Polyaniline nanostructure. *Inorg. Chem. Commun.* **2023**, *157*. [CrossRef]
15. Turkten, N.; Karatas, Y.; Bekbolet, M. Preparation of PANI Modified ZnO Composites via Different Methods: Structural, Morphological and Photocatalytic Properties. *Water* **2021**, *13*, 1025. [CrossRef]
16. Dakshayini, B.; Reddy, K.R.; Mishra, A.; Shetti, N.P.; Malode, S.J.; Basu, S.; Naveen, S.; Raghu, A.V. Role of conducting polymer and metal oxide-based hybrids for applications in ampereometric sensors and biosensors. *Microchem. J.* **2019**, *147*, 7–24. [CrossRef]
17. Abdah, M.A.A.M.; Azman, N.H.N.; Kulandaivalu, S.; Sulaiman, Y. Review of the use of transition-metal-oxide and conducting polymer-based fibres for high-performance supercapacitors. *Mater. Des.* **2020**, *186*, 108199. [CrossRef]
18. Zenasni, M.; Quintero-Jaime, A.; Benyoucef, A.; Benghalem, A. Synthesis and characterization of polymer/V_2O_5 composites based on poly(2-aminodiphenylamine). *Polym. Compos.* **2021**, *42*, 1064–1074. [CrossRef]
19. Babel, V.; Hiran, B.L. A review on polyaniline composites: Synthesis, characterization, and applications. *Polym. Compos.* **2021**, *42*, 3142–3157. [CrossRef]
20. Zak, A.K.; Abrishami, M.E.; Majid, W.A.; Yousefi, R.; Hosseini, S. Effects of annealing temperature on some structural and optical properties of ZnO nanoparticles prepared by a modified sol–gel combustion method. *Ceram. Int.* **2011**, *37*, 393–398. [CrossRef]
21. Benykhlef, S.; Bekhoukh, A.; Berenguer, R.; Benyoucef, A.; Morallon, E. PANI-derived polymer/Al_2O_3 nanocomposites: Synthesis, characterization, and electrochemical studies. *Colloid Polym. Sci.* **2016**, *294*, 1877–1885. [CrossRef]
22. Gong, C.-L.; Li, Y.-F.; Yang, H.-X.; Wang, X.-L.; Zhang, S.-J.; Yang, S.-Y. Characterization and thermal stability of PMR polyimides using 7-oxa-bicyclo[2,2,1]hept-5-ene-2, 3-dicarboxylic anhydride as end caps. *Chin. J. Polym. Sci.* **2011**, *29*, 741–749. [CrossRef]
23. Khamngoen, K.; Paradee, N.; Sirivat, A. Chemical oxidation polymerization and characterization of poly ortho-anisidine nanoparticles. *J. Polym. Res.* **2016**, *23*, 172. [CrossRef]
24. Deshmukh, M.A.; Patil, H.K.; Bodkhe, G.A.; Yasuzawa, M.; Koinkar, P.; Ramanaviciene, A.; Shirsat, M.D.; Ramanavicius, A. EDTA-modified PANI/SWNTs nanocomposite for differential pulse voltammetry based determination of Cu(II) ions. *Sens. Actuators B Chem.* **2018**, *260*, 331–338. [CrossRef]
25. Dhanalakshmi, J.P.; Raj, M.A.; Vijayakumar, C.T. Thermal degradation kinetics of structurally diverse poly(bispropargyl ethers-bismaleimide) blends. *Chin. J. Polym. Sci.* **2016**, *34*, 253–267. [CrossRef]
26. Butoi, B.; Groza, A.; Dinca, P.; Balan, A.; Barna, V. Morphological and structural analysis of polyaniline and poly(*o*-anisidine) layers generated in a DC glow discharge plasma by using an oblique angle electrode deposition configuration. *Polymers* **2017**, *9*, 732. [CrossRef]
27. Du, X.; Xu, Y.; Xiong, L.; Bai, Y.; Zhu, J.; Mao, S. Polyaniline with high crystallinity degree: Synthesis, structure, and electrochemical properties. *J Appl. Polym. Sci.* **2014**, *131*. [CrossRef]
28. Rajakani, P.; Vedhi, C. Electrocatalytic properties of polyaniline–TiO_2 nanocomposites. *Int. J. Ind. Chem.* **2015**, *6*, 247–259. [CrossRef]
29. Han, J.-C.; Wang, S.-F.; Deng, R.; Wu, Q.-Y. Polydopamine/Imogolite Nanotubes (PDA/INTs) Interlayer Modulated Thin Film Composite Forward Osmosis Membrane For Minimizing Internal Concentration Polarization. *Chin. J. Polym. Sci.* **2022**, *40*, 1233–1241. [CrossRef]
30. Norouzian, R.-S.; Lakouraj, M.M.; Zare, E.N. Novel conductive PANI/hydrophilic thiacalix[4]arene nanocomposites: Synthesis, characterization and investigation of properties. *Chin. J. Polym. Sci.* **2014**, *32*, 218–229. [CrossRef]
31. Wang, Y.; Jing, X. Formation of Polyaniline Nanofibers: A Morphological Study. *J. Phys. Chem. B* **2008**, *112*, 1157–1162. [CrossRef] [PubMed]
32. Rangel-Olivares, F.R.; Arce-Estrada, E.M.; Cabrera-Sierra, R. Synthesis and characterization of polyaniline-based polymer nanocomposites as anti-corrosion coatings. *Coatings* **2021**, *11*, 653. [CrossRef]
33. Sozeri, H.; Kurtan, U.; Topkaya, R.; Baykal, A.; Toprak, M. Polyaniline (PANI)–Co0.5Mn0.5Fe2O4 nanocomposite: Synthesis, characterization and magnetic properties evaluation. *Ceram. Int.* **2013**, *39*, 5137–5143. [CrossRef]
34. Salih, R.A. Synthesis, identification and study of electrical conductivity of the doped poly aniline. *Arab. J. Chem.* **2010**, *3*, 155–158. [CrossRef]
35. Xia, Y.; Wiesinger, J.M.; MacDiarmid, A.G.; Epstein, A.J. Camphorsulfonic Acid Fully Doped Polyaniline Emeraldine Salt: Conformations in Different Solvents Studied by an Ultraviolet/Visible/Near-Infrared Spectroscopic Method. *Chem. Mater.* **1995**, *7*, 443–445. [CrossRef]
36. Neetika, M.; Rajni, J.; Singh, P.K.; Bhattacharya, B.; Singh, V.; Tomar, S. Synthesis and properties of polyaniline, poly(*o*-anisidine), and poly[aniline-co-(*o*-anisidine)] using potassium iodate oxidizing agent. *High Perform. Polym.* **2016**, *29*, 266–271. [CrossRef]

37. Rannou, P.; Gawlicka, A.; Berner, D.; Pron, A.; Nechtschein, M.; Djurado, D. Spectroscopic, Structural and Transport Properties of Conductive Polyaniline Processed from Fluorinated Alcohols. *Macromolecules* **1998**, *31*, 3007–3015. [CrossRef]
38. Alam, M.; Alandis, N.M.; Ansari, A.A.; Shaik, M.R. Optical and Electrical Studies of Polyaniline/ZnO Nanocomposite. *J. Nanomater.* **2013**, *2013*, 157810. [CrossRef]
39. Raotole, M.L.; Vaidya, A.M.; Raotole, P.M. Systematic Study of Synthesis of Poly(O-Anisidine-Co-O-Toluidine) Coatings and Its Performance Against Corrosion of Copper. *IJARIIT* **2018**, *104*, 252–260.
40. Basnayaka, P.A.; Ram, M.K.; Stefanakos, E.K.; Kumar, A. Supercapacitors based on graphene–polyaniline derivative nanocomposite electrode materials. *Electrochim. Acta* **2013**, *92*, 376–382. [CrossRef]
41. Begum, B.; Bilal, S.; Shah, A.U.H.A.; Röse, P. Physical, Chemical, and Electrochemical Properties of Redox-Responsive Polybenzopyrrole as Electrode Material for Faradaic Energy Storage. *Polymers* **2021**, *13*, 2883. [CrossRef]
42. Radja, I.; Djelad, H.; Morallon, E.; Benyoucef, A. Characterization and electrochemical properties of conducting nanocomposites synthesized from p-anisidine and aniline with titanium carbide by chemical oxidative method. *Synth. Met.* **2015**, *202*, 25–32. [CrossRef]
43. Lu, Q.; Lee, J.-H.; Lee, J.H.; Choi, H.J. Magnetite/Poly(ortho-anisidine) Composite Particles and Their Electrorheological Response. *Materials* **2021**, *14*, 2900. [CrossRef] [PubMed]
44. Ghann, W.; Kang, H.; Sheikh, T.; Yadav, S.; Chavez-Gil, T.; Nesbitt, F.; Uddin, J. Fabrication, Optimization and Characterization of Natural Dye Sensitized Solar Cell. *Sci. Rep.* **2017**, *7*, 41470. [CrossRef] [PubMed]
45. Belhadj, H.; Moulefera, I.; Sabantina, L.; Benyoucef, A. Effects of Incorporating Titanium Dioxide with Titanium Carbide on Hybrid Materials Reinforced with Polyaniline: Synthesis, Characterization, Electrochemical and Supercapacitive Properties. *Fibers* **2022**, *10*, 46. [CrossRef]
46. Benz, D.; Felter, K.M.; Köser, J.; Thöming, J.; Mul, G.; Grozema, F.C.; Hintzen, H.T.; Kreutzer, M.T.; Ommen, J.R.V. Assessing the Role of Pt Clusters on TiO_2 (P25) on the Photocatalytic Degradation of Acid Blue 9 and Rhodamine B. *J. Phys. Chem. C* **2020**, *124*, 8269–8278. [CrossRef]
47. Bhanvase, B.; Kamath, S.; Patil, U.; Patil, H.; Pandit, A.; Sonawane, S. Intensification of heat transfer using PANI nanoparticles and PANI-CuO nanocomposite based nanofluids. *Chem. Eng. Process.-Process. Intensif.* **2016**, *104*, 172–180. [CrossRef]